JOURNAL OF AIRCRAFT
Vol. 31, No. 2, March–April 1994

Time Simulation of Flutter with Large Stiffness Changes

M. Karpel*
Technion—Israel Institute of Technology, Haifa, Israel
and
C. D. Wieseman†
NASA Langley Research Center, Hampton, Virginia 23681

Time simulation of flutter, involving large local structural changes, is formulated with a state-space model that is based on a relatively small number of constant generalized coordinates. Vibration modes are first calculated for a nominal finite element model with relatively large fictitious masses located at the area of structural changes. A low-frequency subset of these modes is then transformed into a set of structural modal coordinates with which the entire simulation is performed. These generalized coordinates and the associated oscillatory aerodynamic force coefficient matrices are used to construct an efficient time-domain, state-space model for a basic aeroelastic case. The time simulation can then be performed by simply changing the mass, stiffness, and damping coupling terms when structural changes occur. It is shown that the size of the aeroelastic model required for time simulation with large structural changes at a few a priori known locations is similar to that required for direct analysis of a single structural case. The method is applied to the simulation of an aeroelastic wind-tunnel model. The diverging oscillations are followed by the activation of a tip-ballast decoupling mechanism that stabilizes the system, but may cause significant transient overshoots.

Nomenclature

$[A]$ = system matrix
$[A_1]$, $[A_2]$ = matrix coefficients of aerodynamic approximation
$[B]$ = damping matrix of nominal structure
b = reference semichord
$[C]$ = output matrix
$[D]$, $[E]$ = matrix coefficients of aerodynamic approximation
$[GB]$ = generalized structural damping matrix
$[GK]$ = generalized structural stiffness matrix
$[GM]$ = generalized structural mass matrix
$[I]$ = identity matrix
$[K]$ = stiffness matrix of nominal structure
k = reduced frequency, $\omega b/V$
$[M]$ = mass matrix of nominal structure
$[M_f]$ = matrix of fictitious masses added to nominal structure
m = number of aerodynamic roots
n = number of degrees of freedom in finite element model
n_f = number of modes with fictitious masses taken into account for aeroelastic modeling
$[Q(ik)]$ = generalized aerodynamic force coefficient matrix
$[\bar{Q}_b(\bar{s})]$ = approximated generalized aerodynamic force matrix
q = dynamic pressure
$[R]$ = diagonal aerodynamic lag matrix
s = Laplace variable
$\bar{s}$ = nondimensionalized Laplace variable, sb/V
t = time
V = true airspeed
$\{x\}$ = discrete structural displacement vector
$\{x_a\}$ = aerodynamic state vector
$\{y\}$ = vector of outputs
$[\Delta B]$ = change in damping matrix
$[\Delta K]$ = change in stiffness matrix
$[\Delta M]$ = change in mass matrix
$[\zeta]$ = diagonal modal damping coefficient matrix
λ = eigenvalues of A
$\{\xi\}$ = generalized displacements
$[\phi]$ = matrix of vibration modes in discrete coordinates
$[\chi]$ = undamped eigenvectors in modal coordinates
$[\psi]$ = eigenvectors of A
ω = vibration frequency
ω_n = natural vibration modal frequency
$[\omega_n]$ = diagonal matrix of natural frequencies

Subscripts

a = actual case of stiffness variation
accl = accelerations
b = basic structural modes
d = direct model
disp = displacements
F = flutter
f = fictitious masses
r = response locations
T = transition in stiffness
vel = velocities

Received Feb. 11, 1992; presented as Paper 92-2394 at the AIAA/ASME/ASCE/AHS/ASC 33rd Structures, Structural Dynamics and Materials Conference, Dallas, TX, April 13–15 1992; revision received Nov. 2, 1992; accepted for publication Nov. 5, 1992.

*Associate Professor, Faculty of Aerospace Engineering. Member AIAA.

†Aerospace Engineer, Aeroelastic Analysis and Optimization Branch, M/S 246. Member AIAA.

Introduction

THE common approach for formulating the equations of motion of aeroelastic systems starts with a normal modes analysis of the structural model.[1] Unsteady aerodynamic force coefficient matrices are then calculated at various reduced frequency values to account for the aerodynamic coupling

between these modes while undergoing oscillatory motion. Classical frequency-domain aeroelastic analysis methods[2] use the modal structural properties and the tabulated aerodynamic matrices to calculate the flutter conditions at which the aeroelastic system matrix is neutrally stable. The basic assumption of the modal approach is that the structural deflections of the aeroelastic system are linear combinations of a limited set of low-frequency vibration modes.

Time-domain aeroelastic modeling techniques, which transform the equations of motion into a state-space, time-invariant form, call for the approximation of the aerodynamic matrices by rational functions in the Laplace domain. The order of the resulting state-space model is a function of the number of selected modes, the number of aerodynamic approximation roots, and the approximation formula. The main considerations in constructing the model are its size (which affects the efficiency of the subsequent analyses), its accuracy, and the model construction efforts. Tiffany and Adams[3] summarized and extended the most commonly used aerodynamic approximation methods. Among those, the minimum-state (MS) method of Karpel[4-6] yields the smallest state-space aeroelastic models per desired accuracy. Being based on an iterative nonlinear least-square solution, the minimum-state method requires larger model-construction computer time, but the extra time is minor relative to the time savings in typical subsequent analyses.

Time simulation of dynamic response during which structural changes occur requires repeated modifications of the model for numerous structural variations. Repeated calculation of the normal modes and the associated aerodynamic matrices every time the structure changes is often impractical. A more practical approach is to introduce structural changes without changing the modal coordinates. The validity of this approach depends on the structural information contained in the modal coordinates and the magnitude of the structural changes. The number of required modes increases with the magnitude of the allowable structural move limits.

Another advantage of keeping the modal coordinates unchanged is the avoidance of coordinate transformation difficulties. The occurrences of structural changes define the time segments between the model changes. The end conditions of one segment are the initial conditions of the following one. One can argue that these transition-point conditions can be transformed to a set of new coordinates. But this transformation is adequate only if the new coordinates can be expressed as a linear combination of the old ones. However, if this is the case, there is also no need to change the modal coordinates in the first place. An aeroelastic optimization procedure[7] where a realistic wing structure was optimized with aeroservoelastic stability constraints, demonstrated that moderate structural changes can be accommodated without changing the basic 25 modal coordinates. In order to accommodate large structural changes, the modes that serve as generalized coordinates must contain significant distortions in the vicinity of the changes. Taking into account more modes supports this purpose, but may result in an excessively large aeroelastic model.

A method for accommodating large structural changes at a small number of structural locations, without significantly increasing the model size, is presented in Ref. 8. The procedure starts with calculating a set of low-frequency vibration modes with the structure loaded with large fictitious masses at the locations of anticipated structural changes. The fictitious masses cause the vibration modes to contain the local deformations required for an adequate accommodation of large structural changes.

The purpose of this work is to outline the process of applying the fictitious mass (FM) approach to generate efficient fixed-coordinate time-domain aeroelastic models for dynamic response with structural changes, and to demonstrate the use of these models for time simulation of flutter during which large local stiffness changes occur.

Analytical Development

Direct Time-Domain Analysis

Time-domain, first-order, state-space formulation of aeroelastic systems starts (as in the classic second-order, frequency-domain case) with zero-damping normal modes analysis of a finite element model of the flight vehicle. A set of low-frequency vibration modes, $[\phi]$, is then used to calculate the generalized unsteady aerodynamic force (GAF) coefficient matrices, $[Q(ik)]$, for various reduced frequency values. Time-domain modeling requires these GAF matrices to be approximated by rational interpolation functions in the s domain. The aerodynamic approximations in this work are performed by the MS method.[4,5] The approximation function, constrained to exactly match steady aerodynamics, is

$$[\tilde{Q}(\bar{s})] = [Q(0)] + [A_1]\bar{s} + [A_2]\bar{s}^2 + [D](\bar{s}[I] - [R])^{-1}[E]\bar{s} \tag{1}$$

The user defines the $m \times m$ diagonal aerodynamic lag matrix $[R]$ and two additional approximation constraints (for each term), which define the $[A_1]$ and $[A_2]$ matrices as functions of the other coefficients and the tabulated data. The $[D]$ and $[E]$ real coefficient matrices are calculated by an iterative nonlinear least-square procedure that fits the tabulated data matrices. The data terms can be weighted in the least-square process according to their relative importance. The physical weighting algorithm[5,6] used in this work weights the tabulated data according to open-loop aeroelastic response characteristics at a selected dynamic pressure. It has been shown in various applications that the resulting model is applicable to open- and closed-loop analyses with large dynamic pressure variations.[5,6,9,10]

A full description of the state-space aeroservoelastic model resulting from the MS approximation is given in Ref. 11. The state-space equation of motion of the aeroelastic system without external excitation is

$$\{\dot{x}\} = [A]\{x\} \tag{2}$$

where

$$\{x\} = \begin{Bmatrix} \xi \\ \dot{\xi} \\ x_a \end{Bmatrix}$$

$$[A] = \begin{bmatrix} 0 & [I] & 0 \\ -[\bar{M}]^{-1}[\bar{K}] & -[\bar{M}]^{-1}[\bar{B}] & -q[\bar{M}]^{-1}[D] \\ 0 & [E] & (V/b)[R] \end{bmatrix}$$

$$[\bar{M}] = [GM] + \frac{qb^2}{V^2}[A_2]$$

$$[\bar{K}] = [GK] + q[Q(0)]$$

$$[\bar{B}] = [GB] + \frac{qb}{V}[A_1]$$

where the $[GM]$ is found in the normal modes analysis, and $[GK]$ elements are $GK_i = GM_i\omega_{ni}^2$. When the structural damping characteristics are calculated from structural element properties (which is rarely the case), the normal modes are still calculated with zero damping, and the resulting generalized damping matrix is

$$[GB] = [\phi]^T[B][\phi] \tag{3}$$

which is a full matrix. In most cases, however, the generalized damping matrix is assumed to be the diagonal matrix

$$[GB] = 2[\zeta][GM][\omega_n] \tag{4}$$

where $[\zeta]$ is either chosen using engineering judgment (typical values are 0.005–0.02) or measured in a ground vibration test. The dynamic response at specified response locations is related to the response of the states of Eq. (2) by

$$\{y(t)\} = [C]\{x(t)\} \tag{5}$$

where $[C]$ is based on the modal deflections at the response locations, $[\phi_r]$. Structural displacements are calculated with

$$[C_{\text{disp}}] = [\phi_r \quad 0 \quad 0] \tag{6}$$

structural velocities are calculated with

$$[C_{\text{vel}}] = [0 \quad \phi_r \quad 0] \tag{7}$$

and structural accelerations are calculated with

$$[C_{\text{accel}}] = -[\phi_r][\bar{M}]^{-1}[\bar{K} \quad \bar{B} \quad qD] \tag{8}$$

The state response to initial conditions can be expressed analytically as

$$\{x(t)\} = [\psi][e^{\lambda t}][\psi]^{-1}\{x(0)\} \tag{9}$$

where $[e^{\lambda t}]$ is a diagonal matrix where the λ values are the eigenvalues of $[A]$, and $[\psi]$ is the matrix of associated eigenvectors. Most of the eigenvalues and their associated eigenvectors are complex. Since the complex ones appear in conjugate pairs, the resulting $\{x(t)\}$ is always real, and is actually calculated by real-number algebra.

Structural Changes by Direct Modal Coupling

Structural changes that occur during the dynamic response, due to nonlinearities or application of mechanical devices, modify all or some of the finite element $[M]$, $[K]$, and $[B]$ matrices by the increments $[\Delta M]$, $[\Delta K]$, and $[\Delta B]$, respectively. With the assumption that the structural displacements after the changes can still be expressed as linear combinations of the original vibration modes, the analysis can continue with $[GM]$, $[GK]$, and $[GB]$ of Eq. (2) replaced by

$$[GM_a] = [GM] + [\phi]^T[\Delta M][\phi] \tag{10}$$

$$[GK_a] = [GK] + [\phi]^T[\Delta K][\phi] \tag{11}$$

$$[GB_a] = [GB] + [\phi]^T[\Delta B][\phi] \tag{12}$$

The physically weighted aerodynamic approximation performed for the original model is assumed to remain valid for the modified model. This has been demonstrated in stability analysis with moderate[7] and large[8] structural changes.

When the structural changes occur at time $t = t_a$, the state response of Eq. (9) is continued with

$$\{x(t)\} = [\psi_a][e^{\lambda_a(t-t_a)}][\psi_a]^{-1}\{x(t_a)\} \tag{13}$$

where λ_a and $[\psi_a]$ are the eigenvalues and eigenvectors of the modified $[A]$. It should be noted that the modal coordinates do not change when the $[A]$ matrix varies. Consequently, the response coefficient matrix $[C]$ of Eq. (5) remains unchanged, except for that of the acceleration response, Eq. (8), which is now based on Eqs. (10–12).

The flutter characteristics of the system before and after the structural changes are calculated by root-locus analyses of the respective $[A]$ matrices with variable dynamic pressure.

Fictitious Mass Model

The application of the direct modal coupling approach with large structural changes would require the inclusion of a large number of vibration modes. A way to analyze the system stability for large local structural variations with a minimal increase of the model size and without changing the modal coordinates was presented in Ref. 8. The method is extended here to deal with time responses. The finite element vibration modes and the associated GAFs are calculated as above for a nominal case, but with the locations of anticipated structural changes loaded with large fictitious masses. A set of n_f low-frequency fictitious vibration modes, $[\phi_f]$, is selected for further analysis. A coordinate transformation is then performed to "clean out" the fictitious masses and to form an actual "basic" case whose mass and stiffness matrices may differ from those of the nominal case by $[\Delta M_b]$ and $[\Delta K_b]$. The transformation is based on the natural frequencies $[\omega_b]$ and eigenvectors $[\chi_b]$ (normalized to unit generalized masses) associated with the equation of free undamped vibrations in modal coordinates

$$([GM_f] + [\phi_f]^T[\Delta M_b - M_f][\phi_f])\{\ddot{\xi}_f\} + ([GK_f] + [\phi_f]^T[\Delta K_b][\phi_f])\{\xi_f\} = \{0\} \tag{14}$$

The development of Eq. (14) and explanation of its various terms are given in Ref. 8.

The mode shapes and GAFs calculated for the fictitious mass (FM) finite element model are transformed to the basic case by

$$[\phi_b] = [\phi_f][\chi_b] \tag{15}$$

$$[Q_b(ik)] = [\chi_b]^T[Q_f(ik)][\chi_b] \tag{16}$$

The basic-case mode shapes $[\phi_b]$ serve as a constant set of structural generalized coordinates throughout the response analysis (as was $[\phi]$ in the direct modal approach). When the columns of $[\phi_b]$ and the associated frequencies $[\omega_b]$ are compared to those calculated directly for the basic-case finite element model, they appear in two groups. The low-frequency group of n_d modes is practically identical to the directly calculated modes. The $n_f - n_d$ modes in the high-frequency group, whose number and nature depend on the number and magnitudes of the fictitious masses, do not represent actual normal modes, but are synthetic modes with relatively large local distortions in the vicinity of the fictitious masses. In this way, the modes contain detailed local structural information with a minimal increase of the number of modes.

The MS approximation of Eq. (1) is now calculated with the transformed modal data, the state-space Eq. (2) and the acceleration response matrix (8) are constructed for the basic case with $[GM] = [I]$, $[GK] = [\omega_b]^2$ and $[GB] = 2[\zeta_b][\omega_b]$ (in the case of diagonal generalized damping). When the structural damping characteristics are calculated from structural element properties, $[GB_f]$ is first calculated from the FM finite element model using Eq. (3) with $[\phi] = [\phi_f]$, and then transformed to the basic case in the same way the GAF matrices are transformed in Eq. (16).

Most of the response analysis from this point on is performed in the way shown above for the direct modal approach, Eqs. (9–13), with $[\phi] = [\phi_b]$. An exception is the generalized damping matrix $[GB_a]$ of Eq. (12), when large mass and/or stiffness changes appear in Eqs. (10) and (11). With no damping changes, $[GB_a]$ would remain diagonal, but would cause, in effect, damping coupling between the normal modes of the modified system.[8] In order to yield an effectively diagonal structural damping matrix, $[GB]$ is replaced by

$$[GB_a] = 2[GM_a][\chi_a][\zeta_a][\omega_a][\chi_a]^T[GM_a] \tag{17}$$

where $[\omega_a]$ and $[\chi_a]$ are the complete set of frequencies and eigenvectors associated with

$$[GM_a]\{\ddot{\xi}_b\} + [GK_a]\{\xi_b\} = \{0\} \tag{18}$$

Table 1 Natural frequencies of the coupled model

Mode	Direct from NASTRAN	From decoupled with FM	From decoupled without FM	Description
1	0	0	0	Rigid-body roll
2	7.023	7.024	7.032	First fuselage bending
3	7.856	7.864	7.980	First wing bending
4	13.069	13.179	15.413	Ballast pitch
5	16.161	16.134	16.430	Second fuselage bending
6	27.408	27.410	27.467	Third wing bending
7	38.271	38.300	38.761	First wing torsion

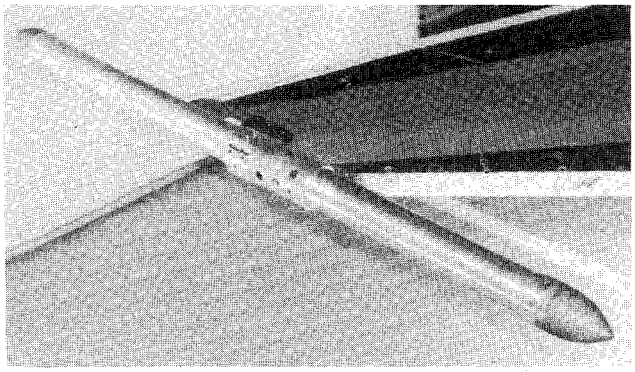

Fig. 1 Close-up view of the AFW wind-tunnel model with tip ballast attachment.

where $[\chi_a]$ is normalized to yield

$$[\chi_a]^T[GM_a][\chi_a] = [I] \tag{19}$$

The accuracy of the FM aeroelastic model (which is based on n_f modes) can be evaluated by separate comparisons of time responses of several structural variations to those obtained directly with their own n_d natural modes. Since the FM models contain more structural information, the structural initial conditions have to be defined first in terms of the coordinates of the direct models. With $\{\xi_d(0)\}$ and $\{\dot{\xi}_d(0)\}$ being the direct-model displacement and velocity initial conditions of a comparison case, the equivalent initial conditions in the associated FM case are

$$\{\xi_f(0)\} = [\bar{\chi}_a]\{\xi_d(0)\} \tag{20}$$

$$\{\dot{\xi}_f(0)\} = [\bar{\chi}_a]\{\dot{\xi}_d(0)\} \tag{21}$$

where the columns of the $n_f \times n_d$ transformation matrix $[\bar{\chi}_a]$ are the n_d lowest-frequency eigenvectors associated with free FM modal equation of motion (18) for this case.

Results

The numerical example consists of a mathematical model of the active flexible wing (AFW) wind-tunnel model[12,13] tested at the NASA Langley Research Center. An external ballast is connected to the tip of the wing through a mechanism designed to decouple the pitch motion of the ballast from that of the wing when flutter occurs. Figure 1 shows a close-up view of the ballast and its attachment to the wing. Details of the structural and aerodynamic models are given in Ref. 8. A frequency-domain flutter analysis by the *p-k* method[2] showed that with "stiff" or "coupled" pitch connection, the Mach 0.9 antisymmetric flutter dynamic pressure is about 1.9 psi and the flutter frequency is about 12 Hz. When the decoupling mechanism is activated, the pitch connection stiffness is reduced by 96.5% ("soft" or "decoupled") and the flutter dynamic pressure changes to about 3 psi and the flutter frequency to 31 Hz. The decoupling device therefore provides a drastic change in both flutter dynamic pressure and the flutter mechanism.

Three time-domain aeroelastic models, starting from separate NASTRAN normal modes analyses, were constructed. Two were direct coupled and decoupled models, and the third was an FM model. The generalized aerodynamic force coefficient matrices in each case were calculated at 14 reduced frequency values between 0–1.5. Minimum-state, physically weighted rational function approximations of the unsteady aerodynamics[5] were performed with 8 lag terms, which yielded 8 aerodynamic augmenting states. The physical weightings were performed at $q = 1.5$ psi. Each model had two versions, one where the approximation was constrained to match the real and imaginary parts of the aerodynamic data at $k = 1.5$, and one with the real data matching constraint replaced by $[A_2] = 0$ in Eq. (1), to avoid repetitive inversions of $[\bar{M}]$ in Eq. (2). All the models were constructed with diagonal modal damping values of $\zeta = 0.01$.

The FM NASTRAN model was with the decoupled pitch connection and with a fictitious pitch inertia of 3 lb-in.-s^2, twice that of the tip ballast, loading the wing end of the connection pitch spring. A set of 14 low-frequency fictitious mass modes, $[\phi_f]$, was used to generate the basic coupled model by solving for the natural frequencies and eigenvectors of Eq. (14), with $[\Delta M_b] = 0$ in our case, then transforming the data to the coupled modal coordinates, Eqs. (15) and (16), and then performing the aerodynamic approximation and the model construction. A comparison between the first seven natural frequencies of the coupled model obtained directly from NASTRAN, those calculated from the 14 fictitious-mass modes and those calculated by direct coupling from 14 decoupled modes without fictitious masses, is given in Table 1. It is clear that the FM model produces accurate frequencies. The flutter-critical ballast pitch frequency, obtained from the decoupled model without fictitious mass, is 18% higher than the correct one, which indicates that the direct coupling approach is not adequate in our case.

The basic FM aeroelastic model was used for various stability and time-response analyses with different pitch connection stiffnesses between coupled and decoupled conditions. The transition from the basic coupled case to another case is performed by simply introducing the appropriate stiffness and damping coupling terms. A comparison between flutter conditions calculated by the frequency domain *p-k* method and those obtained from root-locus analyses of the state-space models is given in Table 2. The largest deviation of state-space from *p-k* results is in the flutter dynamic pressure of the decoupled FM model with $[A_2] = 0$. The contributors to this error are the large difference between the flutter dynamic pressure (3.102 psi) and the physical weighting dynamic pressure (1.5 psi), the large deviation from the weighting coupled pitch spring, and the $[A_2] = 0$ constraint. The error, however, is still below 5%.

A root-loci plot of the low-frequency eigenvalues of $[A]$, where the pitch connection stiffness is varied in small increments from coupled to decoupled values at $q = 2$ psi, is shown in Fig. 2. This was accomplished by varying $[A]$ from coupled to decoupled linearly. The linear variations are valid because $[\bar{M}]$ in Eqs. (2) and (8) is not affected by the changes. It should be mentioned that with linear variations, while the extreme points modal dampings produced by the application

Table 2 Flutter results with different models

Store connection	Coupled		Decoupled	
Flutter parameter	q_F, psi	ω_F, Hz	q_F, psi	ω_F, Hz
p-k				
Direct (13 modes)	1.889	11.88	2.958	30.88
State space				
Direct (13 modes) with [*A*2]	1.884	11.88	3.018	30.92
Direct (13 modes) with [*A*2] = 0	1.896	11.88	2.985	30.81
FM (14 modes) with [*A*2]	1.918	11.94	3.077	30.94
FM (14 modes) with [*A*2] = 0	1.904	11.96	3.102	30.88

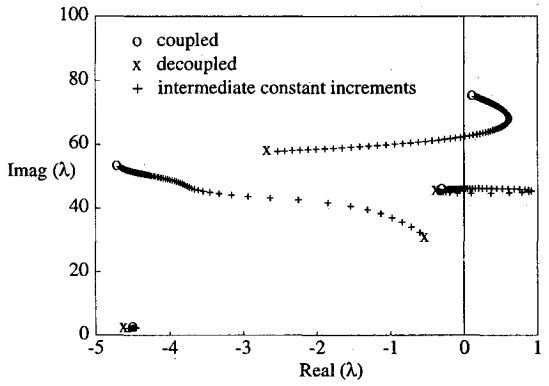

Fig. 2 Root locus of low-frequency eigenvalues of [*A*] from coupled to decoupled.

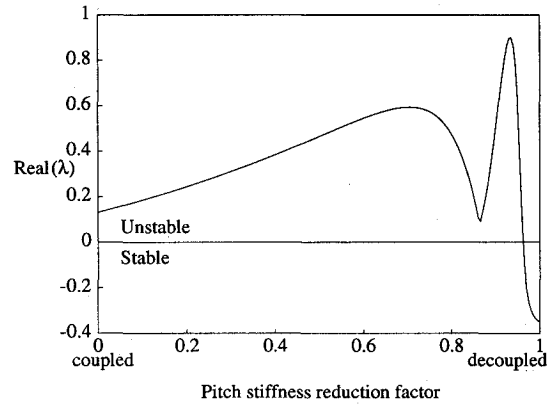

Fig. 3 Maximum real part of eigenvalues with change in stiffness from coupled to decoupled.

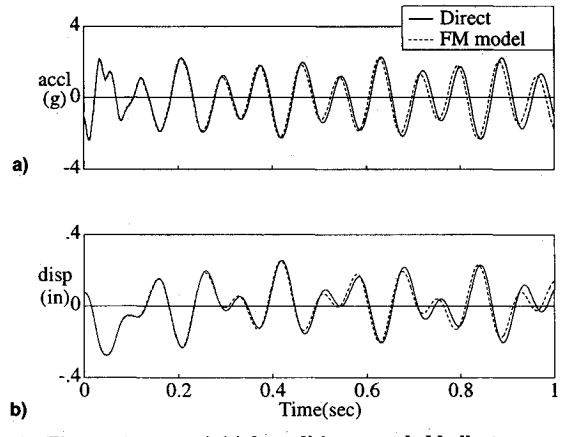

Fig. 4 Time response to initial condition, coupled ballast connection: a) acceleration near the forward end of tip ballast and b) displacement near the forward end of tip ballast.

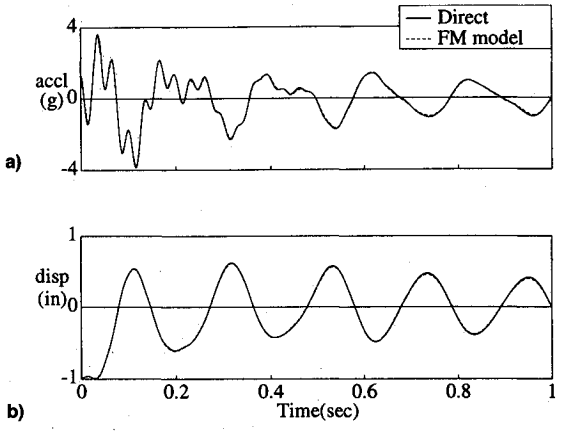

Fig. 5 Time response to initial condition, decoupled ballast connection: a) acceleration near the forward end of tip ballast and b) displacement near the forward end of tip ballast.

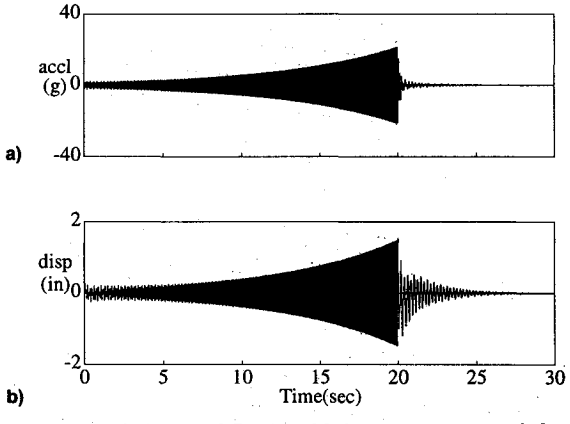

Fig. 6 Time simulation of flutter with instantaneous coupled-to-decoupled transition: a) acceleration near the forward end of tip ballast and b) displacement near the forward end of tip ballast.

of Eq. (17) are effectively diagonal, those at intermediate points are not. However, without having specific knowledge on the damping behavior of the decoupling mechanism at intermediate points, the linear change is as good as other possible variations. The variation of the maximal real part of the eigenvalues of Fig. 2 is shown in Fig. 3. It can be observed that the system stability is very sensitive to the connection spring, especially when it is close to the decoupled conditions. This is an example of important parametric studies that can be performed very efficiently with FM models.

The adequacy of the FM model for time simulation was checked by comparing responses due to initial conditions with those obtained by the direct models. The initial condition chosen was a generalized deflection of 0.1 in the first flexible mode which corresponded to the first fuselage bending mode coupled with wing bending in the coupled tip ballast configuration, and the tip ballast pitch mode in the decoupled tip ballast configuration. The responses were calculated at q =

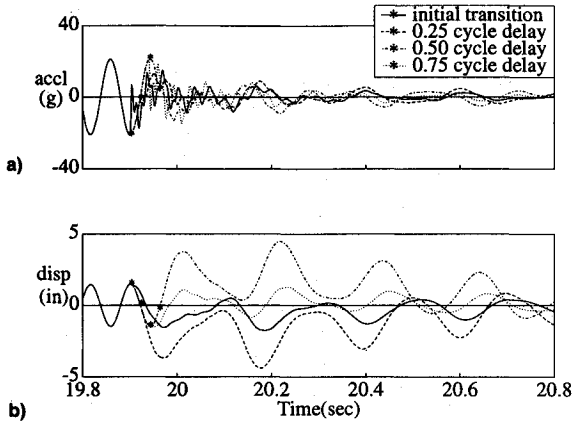

Fig. 7 Time simulation of flutter with instantaneous coupled-to-decoupled transition showing effect of different initiation times: a) acceleration near the forward end of tip ballast and b) displacement near the forward end of tip ballast.

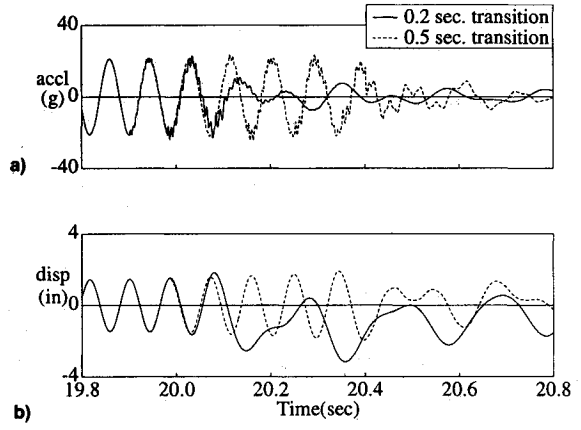

Fig. 8 Time simulation of flutter with gradual coupled to decoupled transition showing effect of different transition times: a) acceleration near the forward end of tip ballast and b) displacement near the forward end of tip ballast.

2 psi, which is about 5% higher than the coupled flutter dynamic pressure and 33% lower than that of the decoupled case. Comparisons were made between the models with $[A_2] = 0$ and between the models with $[A_2]$ not equal to 0. Comparisons are presented for the $[A_2]$ not equal to 0 models only, because the results are similar to those of the $[A_2] = 0$ models. The comparison of the coupled results is shown in Fig. 4 and the comparison of the decoupled results is shown in Fig. 5. The solid line in each of the figures is for the direct model and the dashed line is for the FM-derived model. The vertical acceleration and the displacement at a location on the tip ballast near the forward end are shown. The FM model time histories are very close to those of the direct models, thus validating that the FM model is adequate for time response with large stiffness variations.

A time simulation of flutter with large structural changes was conducted with the FM model at $q = 2$ psi. The starting point was with the coupled model which is slightly unstable. The initial conditions were again a generalized deflection of 0.1 in the first flexible mode. The time-simulation started with a 19.9-s segment of the coupled model. The transition point was arbitrarily chosen to be a peak of the acceleration response near the forward end of the tip ballast. At this point in time, the model was instantaneously changed to the decoupled one, where the end conditions of the first segment served as initial conditions of the second one. A 30-s time simulation is shown in Fig. 6. The time simulation was repeated for different decoupling initiation times. The comparison of the time histories around the transition points is shown in Fig. 7. The time histories are that of Fig. 6 and delays in the transition to decoupled of 0.25, 0.5, and 0.75 cycles. The stars on the figures label the points at which the transitions from coupled to decoupled occurred. It can be observed that, while the level of the acceleration response does not change significantly, the displacement response is very sensitive to the initialization time and may exhibit large overshoots, even though the system becomes stable.

The effect of the amount of time that the system takes to go from coupled to decoupled was also investigated and is shown in Fig. 8. The solid line is for the case when the time of transition is $t_T = 0.2$ s. The dashed line is when the time of transition is $t_T = 0.5$ s. The system is coupled until approximately $t_0 = 19.9$ s, and then the initial stiffness change occurs. In both cases, the $[A]$ matrix varies linearly from coupled, $[A_b]$, to decoupled, $[A_a]$, during the time interval in a stairstep fashion, according to

$$
\begin{aligned}
t < t_0 \quad & [A] = [A_b] \\
t_0 < t < t_0 + \Delta t \quad & [A] = [A_b] - [\Delta A] \\
& \vdots \quad \vdots \\
t_0 + i\Delta t < t < t_0 + (i+1)\Delta t \quad & [A] = [A_b] - (i+1)[\Delta A] \\
& \vdots \quad \vdots \\
t > t_0 + N\Delta t \quad & [A] = [A_a]
\end{aligned}
$$

where

$$\Delta t = t_T/N$$

$$[\Delta A] = ([A_b] - [A_a])/(N+1)$$

where N is the number of time segments. Results were calculated for varying numbers of divisions between coupled and decoupled for both transition time cases. The results are sensitive to the transition time and to the number of divisions between coupled and decoupled for two reasons. The first reason is the sensitivity to time points of stiffness changes as was shown previously in Fig. 7. The second reason is that the least stable root is very sensitive to the stiffness as was shown in Fig. 3. Typical results shown in Fig. 8 are for $N = 10$. The motion of the wing exhibits increased instability in the transition region for both the 0.2- and 0.5-s transition time cases, as expected from the root locus shown in Fig. 2. The maximal displacement overshoots, however, are smaller when the transition time increases, because the stiffness changes are more gradual.

Concluding Remarks

Normal modes calculated with fictitious masses at selected structural locations constitute a set of generalized coordinates with which aeroelastic systems can be analyzed over a wide range of stiffness changes in the vicinity of these locations. The physically weighted minimum-state rational approximation of the unsteady aerodynamic force coefficient matrices is performed only once, for all the stiffness variations. The size of the resulting time-domain model is similar to those required for the analysis of each stiffness case separately. This model facilitates an efficient simulation of aeroelastic time response during which large stiffness changes occur. A numerical application demonstrated a flutter instability followed by rapid stabilization due to the activation of a decoupling mechanism which reduces the stiffness of a critical element by 96.5%. The example indicates that the activation of the decoupler mechanism may cause a transient overshoot before the system stabilizes. The overshoots are highly sensitive to the decoupling initialization time and to the length of transition time.

Acknowledgments

The work presented in this article was supported in part by NASA Grant NAGW-1708, and in part by NASA Contract NAS1-18605 while M. Karpel was at residence at ICASE, NASA Langley Research Center, Hampton, Virginia 23665. This support is gratefully acknowledged.

References

[1]Bisplinghoff, R. L., and Ashley, H., *Principles of Aeroelasticity*, Wiley, New York, 1962, Chap. 9.

[2]Adams, W. M., Jr., Tiffany, S. H., Newsom, J. R., and Peele, E. L., "STABCAR—A Program for Finding Characteristic Roots of Systems Having Transcendental Stability Matrices," NASA TP-2165, June 1984.

[3]Tiffany, S. H., and Adams, W. M., Jr., "Nonlinear Programming Extensions to Rotational Approximation Methods of Unsteady Aerodynamic Forces," NASA TP-2776, July 1988.

[4]Karpel, M., "Design for Active Flutter Suppression and Gust Alleviation Using State-Space Aeroelastic Modeling," *Journal of Aircraft*, Vol. 19, No. 3, 1982, pp. 221–227.

[5]Karpel, M., "Time-Domain Aeroservoelastic Modeling Using Weighted Unsteady Aerodynamic Forces," *Journal of Guidance, Control, and Dynamics*, Vol. 13, No. 1, 1990, pp. 30–37.

[6]Karpel, M., "Extension to the Minimum-State Aeroelastic Modeling Method," *AIAA Journal*, Vol. 29, No. 11, 1991, pp. 2007–2009.

[7]Karpel, M., "Multidisciplinary Optimization of Aeroservoelastic Systems Using Reduced-Size Models," *Journal of Aircraft*, Vol. 29, No. 5, 1992, pp. 939–946.

[8]Karpel, M., and Wieseman, C. D., "Modal Coordinates for Aeroelastic Analysis with Large Local Structural Variations," *Journal of Aircraft*, Vol. 31, No. 2, 1994, pp. 396–403.

[9]Karpel, M., and Hoadley, S. T., "Physically Weighted Approximations of Unsteady Aerodynamic Forces Using the Minimum-State Method," NASA TP-3025, March 1991.

[10]Hoadley, S. T., and Karpel, M., "Application of Aeroservoelastic Modeling Using Minimum-State Unsteady Aerodynamic Approximations," *Journal of Guidance, Control, and Dynamics*, Vol. 14, No. 11, 1991, pp. 1267–1276.

[11]Karpel, M., "Reduced-Order Aeroelastic Models via Dynamic Residualization," *Journal of Aircraft*, Vol. 27, No. 5, 1990, pp. 449–455.

[12]Miller, G. D., "Active Flexible Wing Technology," AFWAL-TR-87-3096, Feb. 1988.

[13]Perry, B. P., III, Cole, S. R., and Miller, G. D., "Summary of the Active Flexible Wing Program," AIAA Paper 92-2080, April 1992.